An Improved Model Predictive Torque Control For PMSM Drives Based on Discrete Space Vector Modulation

Wei Zhang, Yong Yang, *Senior Member, IEEE*, Mingdi Fan, *Senior Member, IEEE*, Liqun He, *Member*, *IEEE*, Aiming Ji, Yang Xiao, *Member, IEEE*, Huiqing Wen, *Senior Member, IEEE*, Xinan Zhang, *Member, IEEE*, Tao Yang, *Senior Member, IEEE*, Saad Mekhilef, *Fellow, IEEE*, Jose Rodriguez, *Life Fellow, IEEE*

***Abstract*—In this paper, an improved model predictive torque control (MPTC) method based on discrete space vector modulation (DSVM) is proposed for permanent magnet synchronous motor (PMSM) drives. Aiming at solving the two problems of large torque ripples and high computational complexity in conventional MPTC, the proposed method adopts a second optimization and a new simplified search strategy. The key idea of second optimization is to make the output voltage vector closer to the actual optimal solution. In this case, a more suitable voltage vector is applied in each sampling period. The simplified search strategy reduces the calculation time by cutting down the number of candidate voltage vectors without affecting drives performance. Compared to the conventional MPTC without DSVM and with DSVM, the proposed method can produce superior steady-state performance and lower computational complexity. Simulation and experimental results are presented to validate the effectiveness and feasibility of the proposed method.**

***Keywords*—Model Predictive Torque Control (MPTC), Permanent Magnet Synchronous Motor (PMSM), Discrete Space Vector Modulation (DSVM).**

I. INTRODUCTION

Field oriented control (FOC) and direct torque control (DTC) are two classical methods for high-performance motor drives [1]-[4]. Compared with FOC, DTC has faster dynamic response, simpler structure and stronger robustness [5]-[6]. The conventional DTC uses two hysteresis comparators for torque and flux control instead of employing the inner loop current regulators. One appropriate voltage vector is directly selected from the switching table without coordinate transformation and pulse-width modulation (PWM) [7]-[8]. Unfortunately, the conventional DTC suffers from the problems of high torque ripples, large current harmonics and variable switching frequency [9]-[11].

To overcome these problems, some advanced control approaches are proposed in recent years, model predictive control (MPC) is an attractive method among them [12]-[16]. One common example is the finite control set based model predictive torque control (FCS-MPTC), which integrates the widely used MPC approach into DTC. The conventional FCS-MPTC can select the optimal voltage vector based on a user-defined cost function, while satisfying the system constraints. Moreover, the parameter robustness of FCS-MPTC is good. Nonetheless, the FCS-MPTC only applies one voltage vector in the entire control cycle, so the high torque and flux ripples still exists [14]-[16].

In order to overcome the drawbacks in conventional FCS-MPTC, many improved methods have been proposed [17]-[18]. These methods can be broadly categorized as hardware based and software based methods. Hardware based methods usually utilize the matrix converters and multi-level converters. For example, predictive controllers for matrix-converter driven interior PMSM (IPMSM) are designed in [17]. The number of output voltage vectors increases drastically when more switches are employed. Experimental results show that the proposed method can achieve good dynamic responses. In [18], some meaningful research is carried out on the four-level hybrid-clamped converter (4L-HCC). Compared with the 8 available voltage vectors in 2-level inverter, the number of candidate voltage vectors in 4L-HCC is 512. Despite the performance improvement, the hardware based methods generally require more sophisticated inverter topology and thus, result in higher cost.

In comparison, the software based methods often focus on the improvement of reference voltage vector synthesis through

Manuscript received September 20, 2022; revised December 13, 2022 ; accepted March 9, 2023. This work was supported in part by the National Natural Science Foundation of China under Grant 51977136, Grant 52277062 and Grant 52007127, in part by the Nature Science Youth Foundation of Jiangsu Province under Grant BK20220499 and in part by projects FB0008, 1210208 and 1221293. (*Corresponding authors*: *Yong Yang; Mingdi Fan*.)

Wei Zhang, Yong Yang, Mingdi Fan, Liqun He, Aiming Ji, Yang Xiao are with the School of Rail Transportation, Soochow University, Suzhou 215131, China (e-mail:wzhang980117@163.com;yangy1981@suda.edu.cn;mdfan@suda.edu.cn;lqhe @ suda.edu.cn; jiaiming@suda.edu.cn; yangxiao@ suda.edu.cn).

Huiqing Wen is with the Electrical and Electronics Department, the Xi'an Jiaotong-Liverpool University, Suzhou 215123, China (e-mail: huiqing.wen@xjtlu.edu.cn).

Xinan Zhang is with the Department of Electrical, Electronic and Computer Engineering, University of Western Australia, Perth, WA 6009, Australia (e-mail: xinan.zhang@uwa.edu.au).

Tao Yang is with the Power Electronics Machines and Control Group, University of Nottingham, Nottingham NG7 2RD, U.K. (e-mail: tao.yang@nottingham.ac.uk).

Saad Mekhilef is with the School of Software and Electrical Engineering, Faculty of Science, Engineering and Technology, Swinburne University of Technology, Victoria, VIC 3122, Australia (e-mail: saad@um.edu.my).

Jose Rodriguez is with Faculty of Engineering, Universidad San Sebastian Santiago, Santiago 8370146, Chile. (e-mail: jose.rodriguezp@uss.cl).

control or modulation [19]-[23]. Among them, two-vector-based FCS-MPTC can be divided into narrow and general concepts according to whether the second vector is a zero vector [19]. The narrow two-vector-based FCS-MPTC uses only a zero vector along with an active vector during each sampling period [20], which is also called duty cycle control. On the other hand, the general two-vector-based FCS-MPTC chooses to use the zero vector or the active vector as the second voltage vector according to the actual needs of the output voltage [21]. The general two-vector-based FCS-MPTC is studied in detail in [22]. From the experimental results, it is concluded that the proposed method obtains better performance with a lower switching frequency compared with narrow two-vector-based FCS-MPTC. In order to further enhance the performance, three-vector-based FCS-MPTC has been proposed in [23] which employs three vectors (active vectors or zero vectors) for the synthesis of reference voltage vector. Compared to two-vector-based FCS-MPTC, three-vector-based FCS-MPTC can obtain much better performance. However, the above methods need to select two or three appropriate voltage vectors and calculate their corresponding time duration in each sampling period, which imposes a large calculation burden on the microprocessor.

Discrete space vector modulation (DSVM) method has been acknowledged as a competitive method for torque ripples reduction in motor drives [24]-[28]. The idea of DSVM is to divide a sampling period into several parts so that a large amount of virtual voltage vectors can be generated [24]. In [25], a deadbeat predictive torque control with discrete space vector modulation is proposed. The number of candidate voltage vectors is increased from 8 to 38. It can be seen from the experimental results that the torque ripples and current harmonics of the proposed method are reduced greatly compared to method without DSVM. In [26] DSVM is extended to six-phase induction motor drives, a more suitable voltage vector is selected to fulfill the torque/flux requirements by utilizing many virtual voltage vectors. However, the main disadvantage of conventional DSVM based FCS-MPTC is a heavy computational burden due to the enumeration of all candidate voltage vectors in one sampling period [27]. Especially, the computational burden increases drastically when the sampling period is divided into four or more, which makes it very difficult to apply DSVM to real-time control applications [28].

In order to reduce the computational time while maintaining the performance of conventional DSVM based FCS-MPTC, several approaches are proposed [29]-[30]. In [29], the number of candidate voltage vectors is reduced from 38 to 3 with the help of deadbeat control method. In [30], the sector determination is added before cost function enumeration. Consequently, the number of candidate voltage vectors is reduced from 38 to 15 without other algorithm cost.

In this paper, an improved MPTC based on DSVM is proposed for PMSM drives. On one hand, for the purpose of

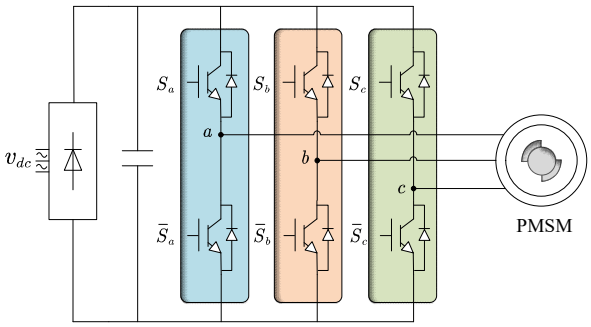

Fig. 1 Scheme of a PMSM drive.

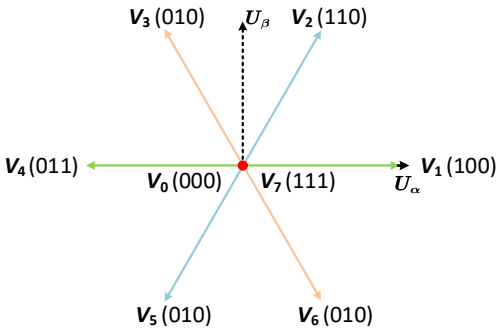

Fig. 2 Basic voltage vectors.

reducing calculation burden, the proposed method adopts a novel flexible searching strategy according to the real-time reference VV changes. To be specific, the location of reference VV is divided into three cases in the adopted searching strategy. The detail of three cases will be discussed in the following section. Compared with the traditional MPTC that needs to iteratively evaluate 38 candidate VVs in the cost function to find out the optimal VV, the proposed method only needs to evaluate 7, 20 and 15 candidate VVs in the afore-mentioned three cases while being able to determine the optimal VV Thus, the computational time is greatly reduced. On the other hand, the proposed method develops second stage optimization based on the virtual voltage vectors generated by DSVM to further improve the steady-state performance of drives. The key to second stage optimization is to make the output voltage vector closer to the reference voltage vector, which results in reduced torque ripples and current harmonics. The feasibility and effectiveness of the proposed method are verified by abundant simulation and experimental tests on a two-level inverter-fed PMSM.

II. Models of System

A. Mathematical Model

The topology of a two-level voltage source inverter driving a PMSM is shown in Fig. 1. The output voltage changes according to different switching states as:

$$V_i = \frac{2}{3} u_{dc} (S_1 + aS_2 + a^2 S_3) \quad (1)$$

where $V_i(i=0,...,7)$ is the terminal voltage applied to PMSM, u_{dc} is dc bus voltage, S_1,S_2,S_3 are the switching states of three bridge arms, and $a=e^{i2\pi/3}$.

Fig. 2 shows the voltage vectors generated by the inverter.

The time domain mathematical model of a PMSM in the rotating *d, q*-reference frame is given as:

$$\begin{cases} u_d = R_s i_d + L_d \dfrac{di_d}{dt} - L_q \omega_e i_q \\ u_q = R_s i_q + L_q \dfrac{di_q}{dt} + L_d i_d \omega_e + \psi_f \omega_e \end{cases} \tag{2}$$

where u_d and u_q are *d, q* -axis stator voltages, i_d and i_q are *d, q* -axis stator currents, R_s is stator winding resistance, L_d and L_q are *d, q* -axis inductances, ω_e is electrical rotor angular velocity, ψ_f is the magnitude of permanent magnet flux linkage.

In order to predict the future behavior, the system model is discretized by using forward Euler equation as:

$$\begin{cases} x(k+1) = Ax(k) + Bu(k) + \varepsilon \\ y(k) = Cx(k) + \phi \end{cases} \tag{3}$$

where $x=[i_d \ i_q]^T, u=[u_d \ u_q]^T, y=[T_e \ \psi_d \ \psi_q]^T$, and

$$A=\begin{bmatrix} 1-\dfrac{R_s T_s}{L_d} & \dfrac{\omega_e T_s L_q}{L_d} \\ -\dfrac{\omega_e T_s L_d}{L_q} & 1-\dfrac{R_s T_s}{L_q} \end{bmatrix}, \ B=\begin{bmatrix} \dfrac{T_s}{L_d} & 0 \\ 0 & \dfrac{T_s}{L_q} \end{bmatrix}$$

$$C=\begin{bmatrix} 0 & \dfrac{3}{2} p\psi_f \\ L_d & 0 \\ 0 & L_q \end{bmatrix}, \ \varepsilon=\begin{bmatrix} 0 \\ -\dfrac{\omega_e T_s \psi_f}{L_q} \end{bmatrix}, \ \phi=\begin{bmatrix} 0 \\ \psi_f \\ 0 \end{bmatrix} \tag{4}$$

where T_s is the sampling period, $i_d(k+1), i_q(k+1)$ are the predictive values of *d, q*-axis currents at instant k+1, $i_d(k), i_q(k)$ are the actual values of *d, q*-axis currents at instant k, $u_d(k), u_q(k)$ are the actual values of *d, q*-axis voltages at instant k, p is the number of pole pairs of the PMSM.

B. Cost Function Design

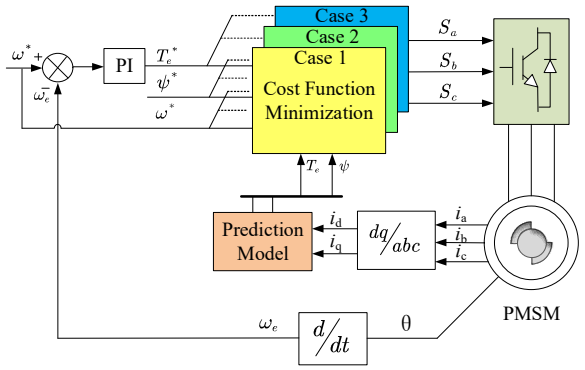

Fig. 3 Control block diagram of proposed method.

Table I

PARAMETER OF PLATFORM

Parameter	Symbol	Numeric Value
Rated speed	ω_{enom}	3000 r/min
Max speed	$W_{\max}$	4500 r/min
Rated torque	T_{enom}	1.27 Nm
d-axis inductances	L_d	6.5 mH
q-axis inductances	L_q	6.5 mH
Stator phase resistance	R_s	2.35 Ω
Sample time	T_s	0.0001 s
Inertia coefficient	J	0.0003 kgm^2
Flux linkage	ψ_f	0.07876 Wb
Max DC Voltage	$u_{dc\max}$	310 V
Pole pairs	p	4
Weighting factor	σ	1265

In FCS-MPTC, the cost function is usually designed as follows:

$$J=(T_e(k+1)-T_e^*)^2+\sigma(\psi(k+1)-\psi^*)^2 \tag{5}$$

where σ is the weighting factor.

The adjustment of the weighting factor has always been a problem in conventional MPTC. In this paper, the value of σ is obtained through a thorough trial and error debugging process. In proposed method, the value of σ is set to 1265.

III. PRINCIPLE OF PROPOSED METHOD

The control block diagram of the proposed method in this paper is shown in the Fig. 3. The implementation process can be divided to three parts. The first part adopts a simplified search strategy to reduce the computational burden. This search strategy changes according to the amplitude of reference voltage vector of different cases. Firstly, the reference voltage vector can be calculated with the constrains of (6) on the basis of system model.

$$\begin{pmatrix} T_e(k+1)=T_e^* \\ \psi(k+1)=\psi^* \end{pmatrix} \rightarrow u_{opt} \tag{6}$$

Then the different cases are categorized in (7)-(9)

$$\text{Case 1:} \quad 0<|u_{opt}|<2u_{dc}/9 \tag{7}$$

$$\text{Case 2:} \quad 2u_{dc}/9<|u_{opt}|<4u_{dc}/9 \tag{8}$$

$$\text{Case 3:} \quad 4u_{dc}/9<|u_{opt}|<2u_{dc}/3 \tag{9}$$

where $|u_{opt}|$ is the amplitude of the reference voltage vector, u_{dc} is the actual DC bus voltage.

The second part is the process of selecting the optimal voltage vector. On the basis of the virtual voltage vectors generated by DSVM, the proposed method performs a second step of optimization. A more suitable voltage vector is selected

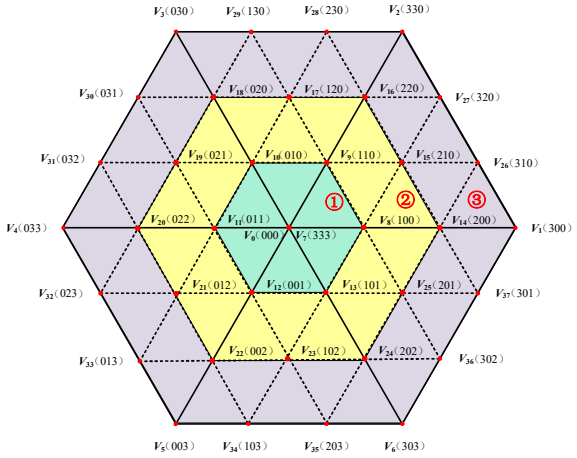

Fig. 4 The description of all candidate voltage vectors.

which can greatly reduce torque ripples and current harmonics, and the control performance is significantly improved.

The third part discusses the determination of radius for virtual range.

In this paper, verification work is carried out in a 2-level inverter PMSM drives. The parameter of platform is shown in Table I. As Table I shown, $u_{dc\max} = 310\ V$.

A. Simplified Search Strategy

Firstly, 38 voltage vectors, including 8 basic voltage vectors

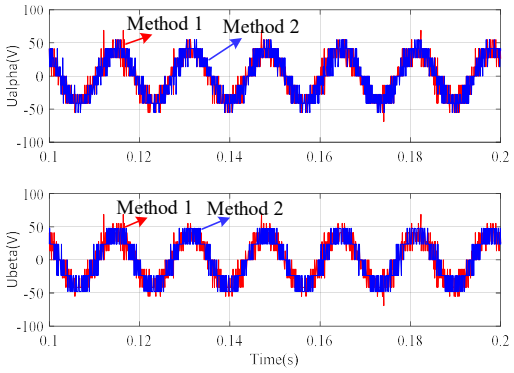

Fig. 5 Comparison of $[u_\alpha, u_\beta]$ of two methods at 900 r/min: Method 1: traditional exhaustive strategy; Method 2: proposed simplified strategy

and 30 virtual voltage vectors, are synthesized via DSVM by dividing each sampling period into three equal parts. The description of virtual voltage vectors is shown in the Fig. 4. In Fig. 4, the vector hexagon is divided into three regions, which correspond to the above three cases. The number "0","1", "2", "3" correspond to the output voltage of 0, $2u_{dc}/9, 4u_{dc}/9, 2u_{dc}/3$, respectively.

The conventional MPTC with DSVM evaluates the cost function for all 38 candidate voltage vectors in one sampling period, which is very time-consuming. In the proposed method, the reference voltage vector can be calculated by PMSM mathematical model. Based on this feature, the simplified searching strategy adopts different strategies to narrow the range of candidate vectors in these three cases. The proposed simplified strategy is compared with the traditional exhaustive search strategy in environment of Matlab/Simulink. The voltage vectors selected by the two methods are compared in Fig. 5. It can be seen that the voltage vectors selected by the two methods are similar validating the proposed simplified search strategy.

Table II

Vectors of different cases

Region	Candidate voltage vectors
①	V_0, V_7, V_8, V_9, V_{10}, V_{11}, V_{12}, V_{13}
②	V_8, V_9, V_{10}, V_{11}, V_{12}, V_{13}, V_{14}, V_{15}, V_{16}, V_{17}, V_{18}, V_{19}, V_{20}, V_{21}, V_{22}, V_{23}, V_{24}, V_{25}
③	V_{15}, V_{17}, V_{19}, V_{21}, V_{23}, V_{25}

Therefore, the simplified search strategy is described as follows.

- In Case 1, only six voltage vectors on the edge of ① and two zero vectors are used for selection. The number of candidate voltage vectors is reduced from 38 to 7.
- In Case 2, using the voltage vectors on the edge of ① and ② for cost function evaluation. The number candidate voltage vectors is reduced from 38 to 20.
- In Case 3, using the voltage vectors on the edge of ② and ③ for prediction. Specially, the optimal sector is identified by evaluating cost function of the central vectors located at the center of six sectors. Then the voltages vectors in one sector are provided. In this case the number of candidate voltage vectors is reduced from 38 to 12.

The candidate voltage vectors in different cases are listed in Table II.

Table III

Vectors of different Sectors in Case 3

Minimum value	Sector	Candidate voltage vectors
V_{15}	I	V_1, V_2, V_{14}, V_{15}, V_{16}, V_{26}, V_{27}
V_{17}	II	V_2, V_3, V_{16}, V_{17}, V_{18}, V_{28}, V_{29}
V_{19},	III	V_3, V_4, V_{18}, V_{19}, V_{20}, V_{30}, V_{31}
V_{21}	IV	V_4, V_5, V_{20}, V_{21}, V_{22}, V_{32}, V_{33}
V_{23}	V	V_5, V_6, V_{22}, V_{23}, V_{24}, V_{34}, V_{35}
V_{25}	VI	V_1, V_6, V_{14}, V_{24}, V_{25}, V_{36}, V_{37}

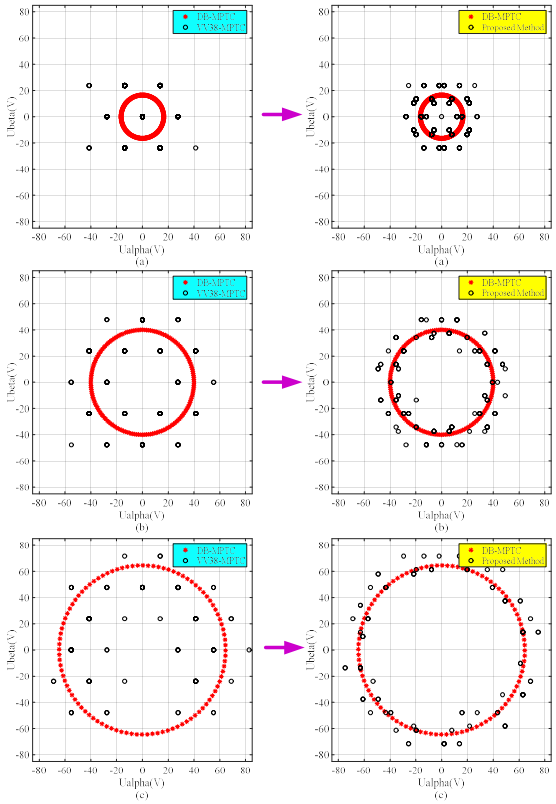

Fig. 6 Comparisons of $\alpha\beta$-axis components of selected voltage vector: (a) 300 r/min; (b) 900 r/min; (c) 1500 r/min

In Case 1 and Case 2, using (5) to calculate the cost function of the voltage vectors in Table II, a suboptimal voltage vector can be obtained:

$$u_{opt1} = arg \min_{①/②} J \tag{10}$$

In particular, in Case 3, the sector selection is performed by (11):

$$Sector = arg \min_{③} J \tag{11}$$

Then, the cost function is evaluated according to the candidate voltage vector corresponding to the selected sector in Table III. A suboptimal voltage vector can be obtained.

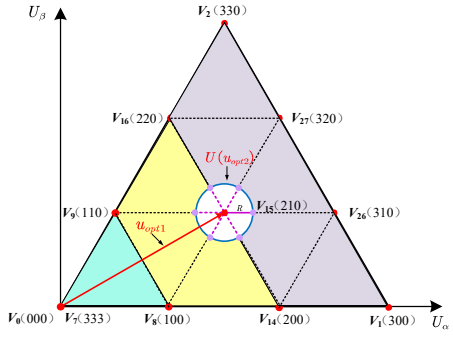

Fig. 7 The schematic diagram of second optimization

Table IV

Vectors after the second optimization

	Candidate voltage vectors
u_{opt1}	$u_{opt1}+R;\ u_{opt1}+\frac{1}{2}R+j\frac{\sqrt{3}}{2}R;$
	$u_{opt1}-\frac{1}{2}R+j\frac{\sqrt{3}}{2}R;\ u_{opt1}-R;$
	$u_{opt1}-\frac{1}{2}R-j\frac{\sqrt{3}}{2}R;\ u_{opt1}+\frac{1}{2}R-j\frac{\sqrt{3}}{2}R$

$$u_{opt1} = arg \min_{Table\ 3} J \tag{12}$$

B. *Optimization Process*

The core idea in optimization process is to equate predicted value and the reference value. This process can be described by:

With u_{opt} and u_{opt1} calculated by part III, the proposed method make comparisons of the $\alpha\beta$-axis components in simulation. The results are shown in Fig. 6. It is visible from the left hand side figures that a clear difference between the two vectors exists in a wide speed range. As shown in Fig. 7, with the u_{opt1} obtained by Part A, in order to reduce the distance between the reference and the selected voltage vectors,

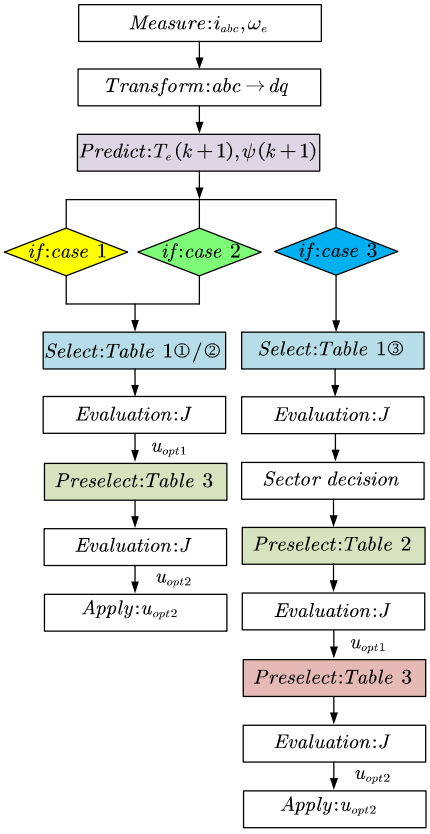

Fig. 8 Algorithm flowchart of proposed method

the proposed method adopts a second stage optimization base on u_{opt1} to synthesize 6 new voltage vectors in a suitably small range. These voltage vectors are used together with u_{opt1} for the second cost function evaluation to obtain the final voltage vector u_{opt2} which will be closer to the reference voltage vector.

Table IV lists the candidate voltage vectors based on u_{opt1}.

The optimal voltage vector can be obtained by:

$$u_{opt2} = arg \min_{Table\ 4} J \tag{14}$$

The right hand side of Fig. 6 shows that the distance between u_{opt2} and the reference voltage vector becomes significantly smaller.

The flowchart of this algorithm is shown in Fig. 8.

C. *Determination of Radius*

The determination of the virtual radius is rarely discussed in recent literature. In this paper, when the amplitude of the reference voltage vector satisfies the region ①, as shown in Fig. 9, the value of virtual radius adopts the radius of the vector circle. And when the amplitude increases to more than half of the side length of the vector hexagon, the inscribed circle of the hexagon and the reference voltage vector circle is made, then the radius of the inscribed circle is adopted as the value of virtual radius. In area ② and area ③, the corresponding virtual radius can be obtained in the similar way. This process can be summarized as:

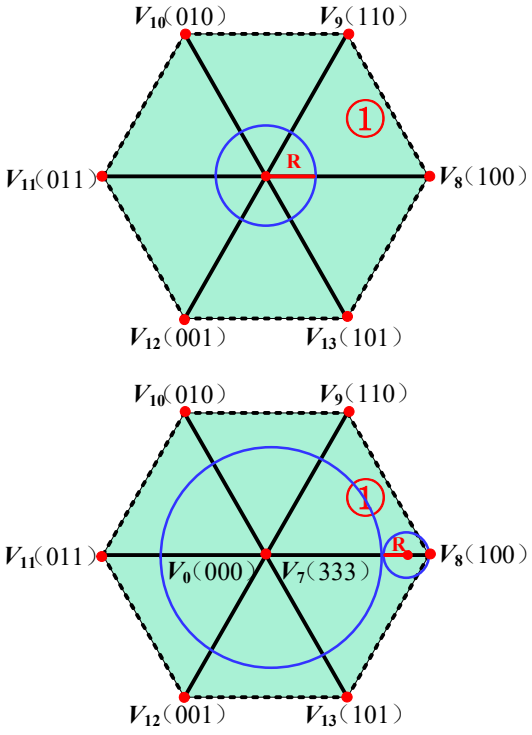

Fig. 9 The determination of virtual radius in region ①.

$$Case\ 1: \begin{cases} R_1 = |u_{opt}| \\ R_2 = \dfrac{1}{3} - R_1 \end{cases} \tag{15}$$

$$Case\ 2: \begin{cases} R_1 = |u_{opt}| - \dfrac{1}{3} \\ R_2 = \dfrac{2}{3} - R_1 \end{cases} \tag{16}$$

$$Case\ 3: \begin{cases} R_1 = |u_{opt}| - \dfrac{2}{3} \\ R_2 = 1 - R_1 \end{cases} \tag{17}$$

where R_1, R_2 are intermediate variables.

The value of radius can be obtained using (18):

$$R = \min\{R_1, R_2\} + R_{base} \tag{18}$$

where R is value of radius. R_{base} is the offset of boundary conditions when $|u_{opt}|$ is $2u_{dc}/9, 4u_{dc}/9, 2u_{dc}/3$. Its value is set to 6% of maximum output voltage to prevent deterioration of control performance.

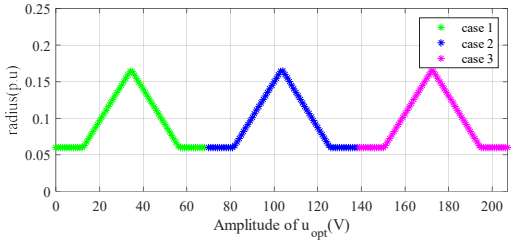

Fig. 10 The value of radius at different cases.

The waveform of the radius is shown in Fig. 10. It can be seen that when the speed is at center of cases, the maximum radius is 0.1667, and the minimum boundary is 0.06 when the speed is at the boundary of cases.

IV. Experimental Results

In this section, the effectiveness of proposed method is tested on the platform in Fig. 11. The microcontroller used to implement the control system is DSP28335. The conditions remain consistent with simulations. In addition, the proposed method is compared with the traditional MPTC, MPTC that employs 38 virtual voltage vectors (VV38-MPTC) under the

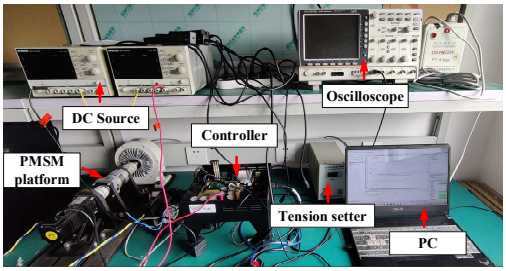

Fig. 11 Test bench

Table V

Execution time of three methods

	Case 1	Case 2	Case 3
Conventional MPTC	4.2μs		
VV38-MPTC	88.0μs		
Proposed method	38.5μs	67.5μs	56.0μs

same conditions. The experimental data are transferred to the PC through a serial port. The switching frequency of three methods is fixed at 10 kHz. The DC bus voltage is set to 124 V. The load torque is set to 0.5 Nm.

A. Computational Time

In order to evaluate the computational burden of the aforementioned three methods, the execution time of the algorithm is measured, including sampling time, coordinate transformation, prediction time, cost function evaluation and etc. The results are shown in Table V.

It can be seen the conventional MPTC has the shortest

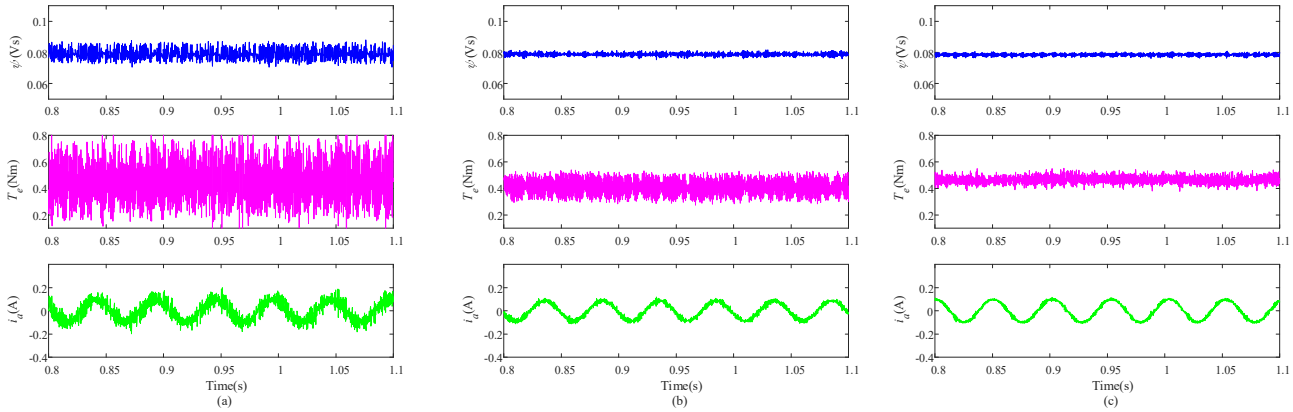

Fig. 12 Steady-state experimental results at 300 r/min of Case 1: (a) Conventional MPTC; (b) VV38-MPTC; (c) Proposed method.

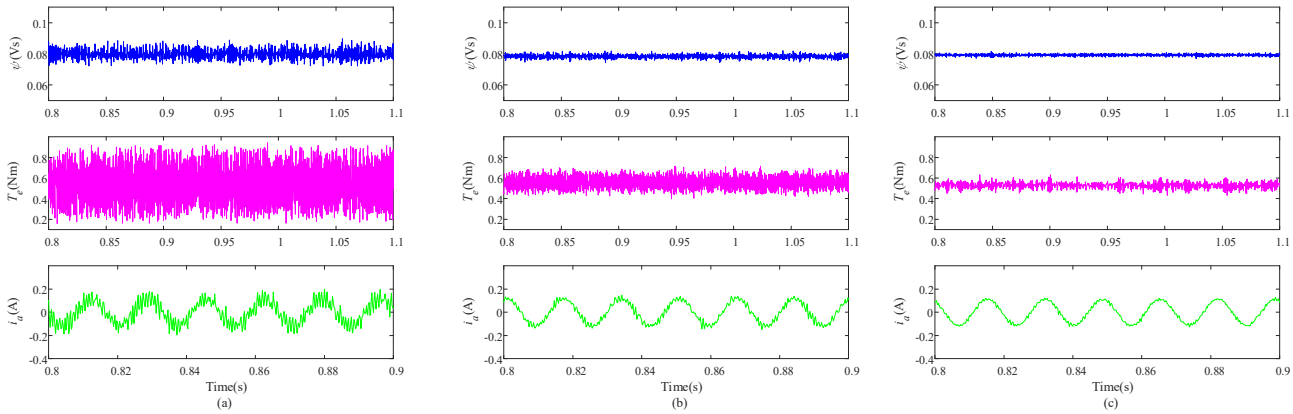

Fig. 13 Steady-state experimental results at 900 r/min of Case 2: (a) Conventional MPTC; (b) VV38-MPTC; (c) Proposed method.

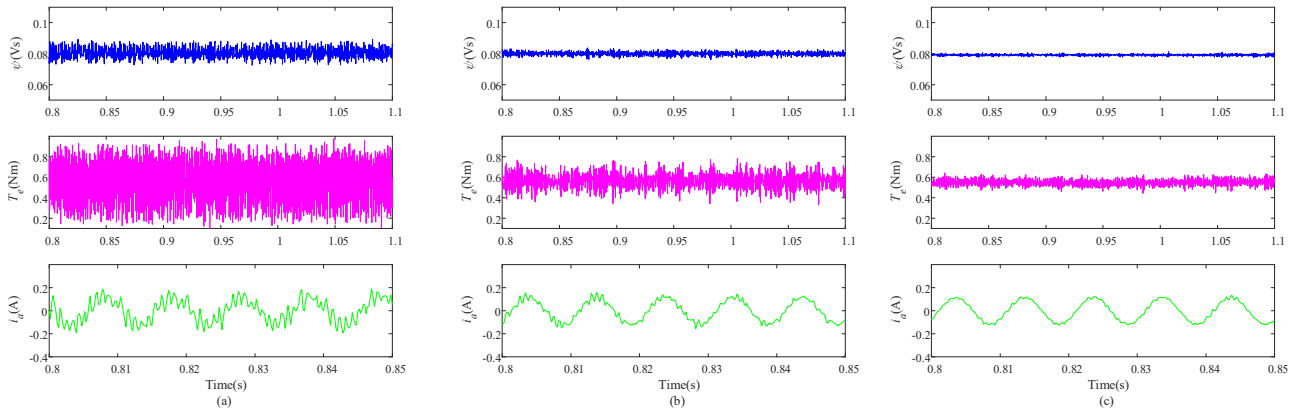

Fig. 14 Steady-state experimental results at 1500 r/min of Case 3: (a) Conventional MPTC; (b) VV38-MPTC; (c) Proposed method.

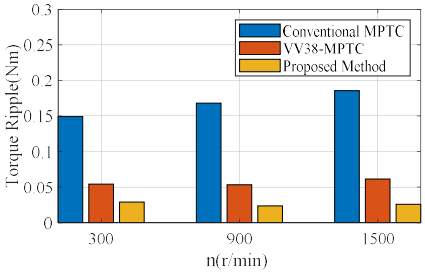

Fig. 15 The RMS of torque ripples of three methods.

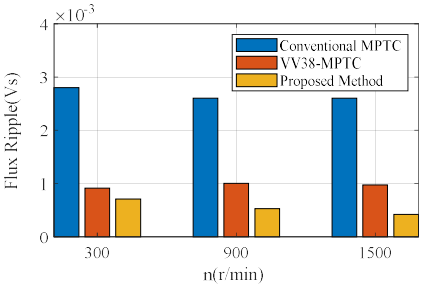

Fig. 16 The RMS of flux ripples of three methods.

execution time due to its simple structure. The execution time of proposed method is significantly lower than that of the VV38-MPTC under different cases.

B. Steady State Performance Analysis

In order to test the steady-state performance of the proposed method in the full speed range, the comparable waveforms of torque, flux linkage and phase A current of three methods at the speeds of 300 r/min, 900 r/min and 1500 r/min are shown in Fig. 12, Fig. 13, and Fig. 14. Moreover, the RMS values of torque and flux linkage ripples and THD of phase current are shown in Fig. 15, Fig. 16 and Fig. 17. Moreover, in order to evaluate the performance of the proposed method in the full

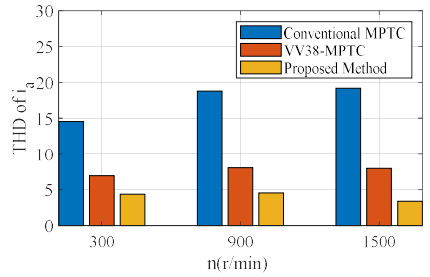

Fig. 17 The THD of phase current of three methods.

speed range. Fig. 18 and Fig. 19 correspond to the experimental waveforms when the motor is reversed and at high speed, respectively.

From these comparative experimental results, it is obvious that the torque and flux ripples of the proposed method are lower than other two methods in the full speed range. And the phase current THD is reduced significantly in the proposed method. This is because the proposed method applies a more suitable voltage vector that is closer to the reference voltage vector.

C. Dynamic Performance Analysis

To assess the dynamic performance of the proposed method, the waveforms are measured in the case of a sudden change in speed from 300 r/min to 900 r/min. The dynamic responses of three methods are shown in Fig.20. It can be seen that all three methods have a fast speed response because they have the same outer speed loop controller.

Except from the sudden change in speed, Fig . 21 shown the waveforms in the case of load change from 0.3Nm to 0.5Nm. It can be seen the proposed contains better performance than other methods.

V. CONCLUSION

In this paper, an improved model predictive torque control (MPTC) method based on discrete space vector modulation (DSVM) is proposed to provide superior performance for

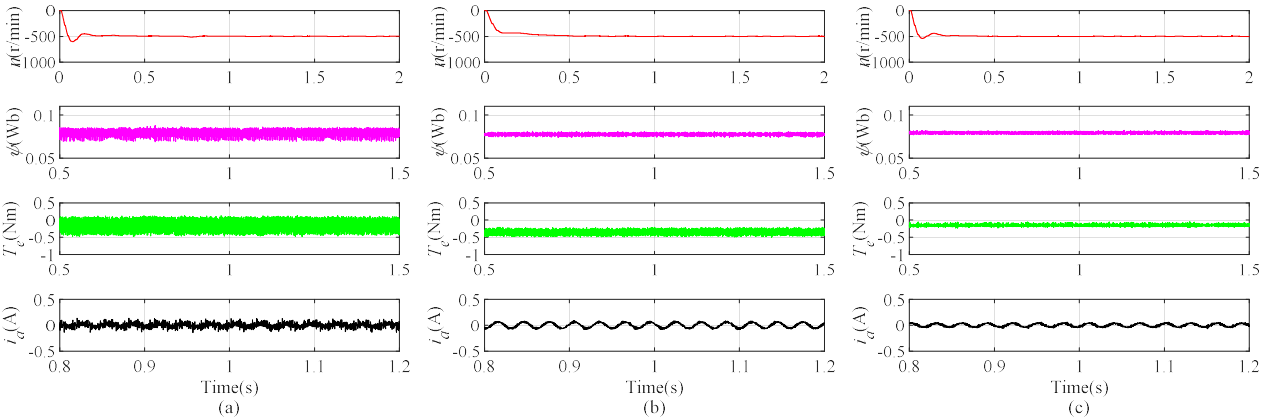

Fig. 18 Steady-state experimental results at -500 r/min of Case 3: (a) Conventional MPTC; (b) VV38-MPTC; (c) Proposed method.

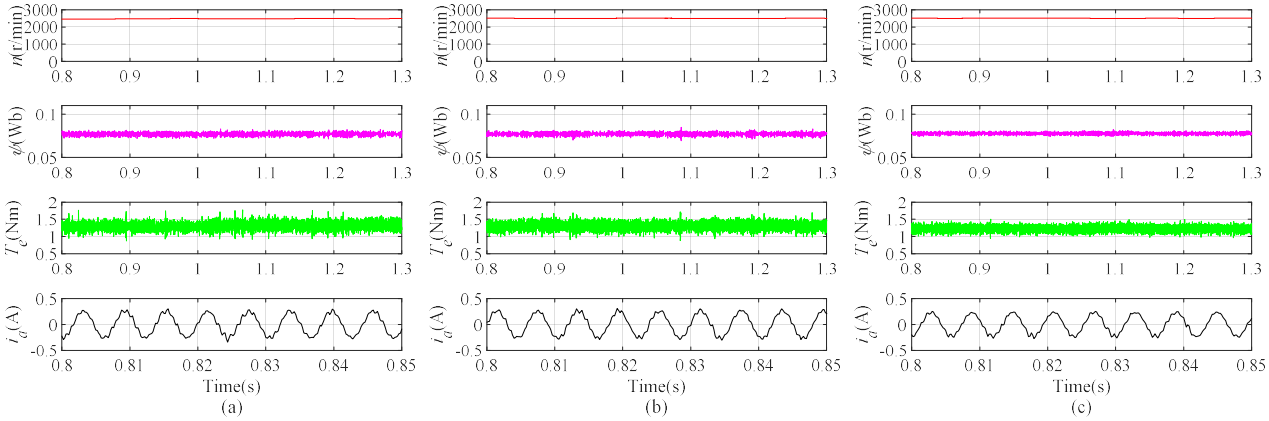

Fig. 19 Steady-state experimental results at 2500 r/min of Case 3: (a) Conventional MPTC; (b) VV38-MPTC; (c) Proposed method.

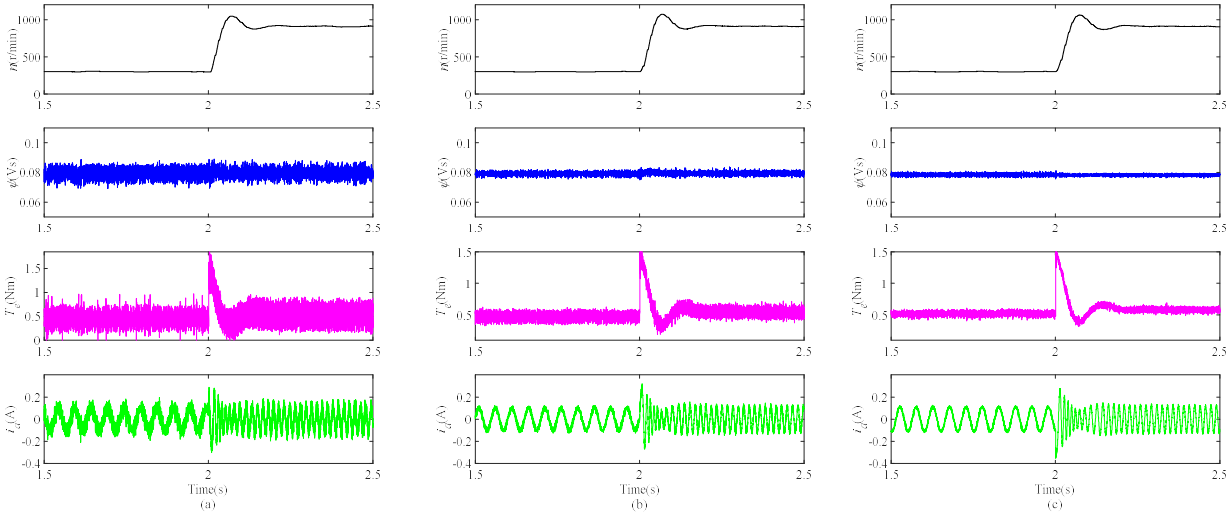

Fig. 20 Dynamic experimental results at 1500 r/min of Case 3: (a) Conventional MPTC; (b) VV38-MPTC; (c) Proposed method.

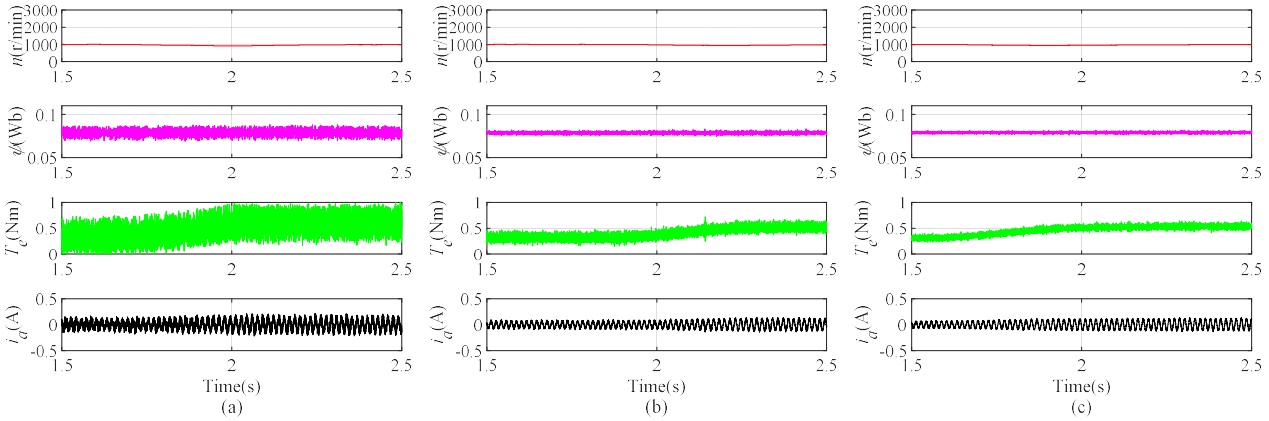

Fig .21 Dynamic experimental results at 1000 r/min of load change: (a) Conventional MPTC; (b) VV38-MPTC; (c) Proposed method.

PMSM drives. Compared to the conventional MPTC with DSVM, the proposed method contributes to substantially diminish the torque/flux ripples and current harmonics in PMSM drives while reducing the computational burden. A new

simplified vector searching strategy is adopted to narrow down the range of candidate voltage vectors based on location of reference voltage vector.

VI. REFERENCES

[1] G. Li, J. Hu, Y. Li and J. Zhu, "An improved model predictive direct torque control strategy for reducing harmonic currents and torque ripples of five-phase permanent magnet synchronous motors," *IEEE Trans. Ind. Electron.,* vol. 66, no. 8, pp. 5820-5829, Aug. 2019.

[2] Y. Luo and C. Liu, "A simplified model predictive control for a dual three-phase PMSM with reduced harmonic currents," *IEEE Trans. Ind. Electron.,* vol. 65, no. 11, pp. 9079-9089, Nov. 2018.

[3] J. Rodriguez et al., "Latest Advances of Model Predictive Control in Electrical Drives—Part I: Basic Concepts and Advanced Strategies," *IEEE Trans. Power Electron.,* vol. 37, no. 4, pp. 3927-3942, April 2022.

[4] W. Zhao, T. Tao, J. Zhu, H. Tan and Y. Du, "A Novel Finite-Control-Set Model Predictive Current Control for Five-Phase PM Motor With Continued Modulation," *IEEE Trans. Power Electron.*, vol. 35, no. 7, pp. 7261-7270, July 2020.

[5] X. Yuan, C. Zhang and S. Zhang, "Torque ripple suppression for open-end winding permanent-magnet synchronous machine drives with predictive current control," *IEEE Trans. Ind. Electron.,* vol. 67, no. 3, pp. 1771-1781, March 2020.

[6] M. S. Mousavi, S. A. Davari, V. Nekoukar, C. Garcia and J. Rodriguez, "A Robust Torque and Flux Prediction Model by a Modified Disturbance Rejection Method for Finite-Set Model-Predictive Control of Induction Motor," *IEEE Trans. Power Electron*., vol. 36, no. 8, pp. 9322-9333, Aug. 2021.

[7] J. Rodriguez et al., "State of the art of finite control set model predictive control in power electronics," *IEEE Trans. Ind. Inform.,* vol. 9, no. 2, pp. 1003-1016, May 2013.

[8] X. Zhang, B. Hou and Y. Mei, "Deadbeat predictive current control of permanent-magnet synchronous motors with stator current and disturbance observer," *IEEE Trans. Power Electron.,* vol. 32, no. 5, pp. 3818-3834, May 2017.

[9] A. A. Ahmed, B. K. Koh and Y. I. Lee, "A comparison of finite control set and continuous control set model predictive control schemes for speed control of induction motors," *IEEE Trans. Ind. Inform.,* vol. 14, no. 4, pp. 1334-1346, April 2018.

[10] Z. Wang, A. Yu, X. Li, G. Zhang and C. Xia, "A Novel Current Predictive Control Based on Fuzzy Algorithm for PMSM," *IEEE J Emerg Sel Top Power Electron*., vol. 7, no. 2, pp. 990-1001, June 2019.

[11] Z. Zhou, C. Xia, Y. Yan, Z. Wang and T. Shi, "Disturbances Attenuation of Permanent Magnet Synchronous Motor Drives Using Cascaded Predictive-Integral-Resonant Controllers," *IEEE Trans. Power Electron*., vol. 33, no. 2, pp. 1514-1527, Feb. 2018.

[12] M. J. Navardi, J. Milimonfared and H. A. Talebi, "Torque and flux ripples minimization of permanent magnet synchronous motor by a predictive-based hybrid direct torque control," *IEEE J Emerg Sel Top Power Electron.,* vol. 6, no. 4, pp. 1662-1670, Dec. 2018.

[13] L. Yan, M. Dou and Z. Hua, "Disturbance compensation-based model predictive flux control of SPMSM with optimal duty cycle," *IEEE J Emerg Sel Top Power Electron.,* vol. 7, no. 3, pp. 1872-1882, Sept. 2019.

[14] Z. Zhou, C. Xia, Y. Yan, Z. Wang and T. Shi, "Disturbances attenuation of permanent magnet synchronous motor drives using cascaded predictive-integral-resonant controllers," *IEEE Trans. Power Electron.,* vol. 33, no. 2, pp. 1514-1527, Feb. 2018.

[15] J. S. Lee, C. Choi, J. Seok and R. D. Lorenz, "Deadbeat-direct torque and flux control of interior permanent magnet synchronous machines with discrete time stator current and stator flux linkage observer," *IEEE Trans. Ind. Appl.,* vol. 47, no. 4, pp. 1749-1758, July-Aug. 2011.

[16] Y. Zhou, H. Li, R. Liu and J. Mao, "Continuous voltage vector model-free predictive current control of surface mounted permanent magnet synchronous motor," *IEEE Trans. Energy Convers.,* vol. 34, no. 2, pp. 899-908, June 2019.

[17] M. S. Mubarok and T. Liu, "Implementation of predictive controllers for matrix-converter-based interior permanent magnet synchronous motor position control systems," *IEEE J Emerg Sel Top Power Electron.,* vol. 7, no. 1, pp. 261-273, March 2019.

[18] Y. Yang et al., "An optimized model predictive control for three-phase four-level hybrid-clamped converters," *IEEE Trans. Power Electron.,* vol. 35, no. 6, pp. 6470-6481, June 2020.

[19] Y. Zhang and J. Zhu, "Direct torque control of permanent magnet synchronous motor with reduced torque ripple and commutation frequency," *IEEE Trans. Power Electron.,* vol. 26, no. 1, pp. 235-248, Jan. 2011.

[20] K. Shyu, J. Lin, V. Pham, M. Yang and T. Wang, "Global minimum torque ripple design for direct torque control of induction motor drives," *IEEE Trans. Ind. Electron.,* vol. 57, no. 9, pp. 3148-3156, Sept. 2010.

[21] W. Chen, S. Zeng, G. Zhang, T. Shi and C. Xia, "A modified double vectors model predictive torque control of permanent magnet synchronous motor," *IEEE Trans. Power Electron.,* vol. 34, no. 11, pp. 11419-11428, Nov. 2019.

[22] Y. Zhang and H. Yang, "Two-vector-based model predictive torque control without weighting factors for induction motor drives," *IEEE Trans. Power Electron.,* vol. 31, no. 2, pp. 1381-1390, Feb. 2016.

[23] S. Chai, L. Wang, and E. Rogers, "A cascade MPC control structure for a PMSM with speed ripple minimization," *IEEE Trans. Ind. Electron.,* vol. 60, no. 8, pp. 2978-2987, 2013.

[24] D. Casadei, G. Serra and K. Tani, "Implementation of a direct control algorithm for induction motors based on discrete space vector modulation," *IEEE Trans. Power Electron.,* vol. 15, no. 4, pp. 769-777, July 2000.

[25] Z. Zhou, C. Xia, Y. Yan, Z. Wang and T. Shi, "Torque ripple minimization of predictive torque control for PMSM with extended control set," *IEEE Trans. Ind. Electron.,* vol. 64, no. 9, pp. 6930-6939, Sept. 2017.

[26] I. M. Alsofyani, S. Kim and K. Lee, "Finite set predictive torque control based on sub-divided voltage vectors of PMSM with deadbeat control and discrete space vector modulation," 2019 IEEE Applied Power Electronics Conference and Exposition (APEC), Mar.2019, pp. 1853-1857.

[27] Y. Wang et al., "Deadbeat model-predictive torque control with discrete space-vector modulation for PMSM drives," *IEEE Trans. Ind. Electron.,* vol. 64, no. 5, pp. 3537-3547, May 2017.

[28] I. Gonzalez-Prieto, M. J. Duran, J. J. Aciego, C. Martin and F. Barrero, "Model predictive control of six-phase induction motor drives using virtual voltage vectors," *IEEE Trans. Ind. Electron.,* vol. 65, no. 1, pp. 27-37, Jan. 2018.

[29] I. Osman, D. Xiao, M. F. Rahman, M. Norambuena and J. Rodriguez, "Discrete space vector modulation based model predictive flux control with reduced switching frequency for IM drive," *IEEE Trans. Energy Convers.,* vol. 36, no. 2, pp. 1357-1367, June 2021.

[30] P. Falkowski, A. Sikorski and M. Malinowski, "Finite control set model predictive control with floating virtual voltage vectors for grid-connected voltage source converter," *IEEE Trans. Power Electron.,* vol. 36, no. 10, pp. 11875-11885, Oct. 2021.

Wei Zhang received the B.S. and M.S. degrees in engineering from Soochow University, Suzhou,China, in 2019 and 2022, respectively.

His research interest includes model predictive control for electric drives

Yong Yang (M'15-SM'20) received the B.S. degree in automation from Xiangtan University, Xiangtan, China, in 2003, the M.S. degree in Electrical Engineering from Guizhou University, Guiyang, China, in 2006, and the Ph.D. degree in Electrical Engineering from Shanghai University, Shanghai, China, in 2010.

He is currently a full Professor with the School of Rail Transportation, Soochow University. From December 2017 to December 2018, he was a Visiting Scholar with Center for High Performance Power Electronics (CHPPE) of The Ohio State University, Columbus, USA. He has coauthored more than 100 journal and conference papers. His current research interests include model predictive control in power electronic converters, distributed energy resource interfacing and high-performance motor drive control.

Mingdi Fan (M'16-SM'20) received B.S. degree in electrical engineering and the Ph.D. degree in detection technology and automation device from Northwestern Polytechnical University, Xi'an, China, in 2008 and 2014. From 2010 to 2011, he worked as a visiting scholar in Kassel University, Germany.

He is currently an Associate Professor with the School of Rail Transportation, Soochow University. His current research interests include model predictive control for power converters and motor drives.

Liqun He (M'19) received the B.E. and Ph.D. degrees from the Huazhong University of Science and Technology (HUST), Wuhan, China, in 2010 and 2015 respectively, all in Electrical Engineering.

She is currently an Associated Professor at the Soochow University, Suzhou, China. Her research interests include fully modular power electronics systems, power electronic transformer, railway electrification, and multi-physics fields of electrical equipment.

Aiming Ji received the B.S. and M.S. degrees in automation from University of Science and Technology Liaoning, Anshan, China, in 1995 and 1999, respectively, and the Ph.D. degree in circuit and system from Zhejiang University, Hangzhou, China, in 2006.

He is currently an Associate Professor with the School of Rail Transportation, Soochow University, Suzhou, China. His current research interests include embedded system and low power design.

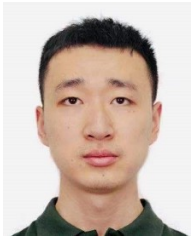

Yang Xiao (S'18-M'20) received the B.Eng., M.Eng. and Ph.D. degrees in Electrical Engineering and Automation, Soochow University, Suzhou, China, and in Electrical Engineering, Southeast University, Nanjing, China, and in Electrical Engineering, City University of Hong Kong, Hong Kong, China, in 2014, 2017 and 2020, respectively.

Currently, Dr. Xiao serves as a Lecturer with the School of Rail Transportation, Soochow University, Suzhou, China. His main research interests include wireless power transmission, battery charger and control of multiphase drive systems.

Huiqing Wen (M'13-SM'19) received his B.S. and M.S. degrees in Electrical Engineering from Zhejiang University, Hangzhou, China, in 2002 and 2006, respectively; and his Ph.D. degree in Electrical Engineering from the Chinese Academy of Sciences, Beijing, China, in 2009. From 2009 to 2010, he was an Electrical Engineer working in the Research and Development Center, GE (China) Co., Ltd., Shanghai, China. From 2010 to 2011, he was an Engineer at the China Coal Research Institute, Beijing, China. From 2011 to 2012, he was a Postdoctoral Fellow at the Masdar Institute of Science and Technology, Abu Dhabi, United Arab Emirates.

He is presently working as a full Professor at the Xi'an Jiaotong-Liverpool University, Suzhou, China. His current research interests include bidirectional DC-DC converters, power electronics in flexible AC transmission applications, electrical vehicles, and high-power, three-level electrical driving systems.

Xinan Zhang (S'10-M'14) received the B.E. degree in electrical engineering and automation from Fudan University, China, in 2008. He received the Ph.D. degree from Nanyang Technological University (NTU), Singapore, in 2014. Then, he worked as postdoc researcher in NTU and the University of New South Wales from 2014 to 2017. He worked as a Lecturer in NTU from June 2017 to September 2019.

Since September 2019, he joined the University of Western Australia as a Senior Lecturer. His research interests include electrical machine drives, control and modulation of power electronic converters and design of hybrid energy storage systems.

Tao Yang (M'16–SM'20) received the M.Eng. degree from Shanghai Jiao Tong University, Shanghai, China, in 2008, and the Ph.D. degree in electrical engineering from the University of Nottingham, Nottingham, U.K., in 2013. Since 2013, he has been a Researcher with the Power Electronics, Machines and Control Group, University of Nottingham, where he became an Assistant Professor in 2016, and an Associate Professor in 2019. His research interests include high-speed electric motor drive control, power electronic conversion, electrical system design and optimization for more electric/hybrid/all-electric aircraft applications. Dr. Yang is currently an Associate Editor for the IEEE TRANSACTIONS ON TRANSPORTATION ELECTRIFICATION and Chinese Journal of Aeronautics. His Ph.D. research within EU Clean Sky on "Modeling electrical power system for more-electric aircraft applications" has resulted in him winning the inaugural "Clean Sky Best Ph.D. Award" in 2016.

Saad Mekhilef (Fellow, IEEE) received the B.Eng. degree in electrical engineering from the University of Setif, Setif, Algeria, in 1995, and the master's degree in engineering science and the Ph.D. degree in electrical engineering from the University of Malaya, Kuala Lumpur, Malaysia, in 1998 and 2003, respectively.

He is currently a Distinguished Professor with the School of Science, Computing and Engineering Technologies, Swinburne University of Technology, Melbourne, VIC, Australia, and an Honorary Professor with the Department of Electrical Engineering, University of Malaya, Kuala Lumpur, Malaysia. He has authored or coauthored more than 500 publications in academic journals and proceedings and 5 books with more than 32 000 citations. His current research interests include power converter topologies, the control of power converters, renewable energy, and energy efficiency.

Jose Rodriguez (M′81-SM′94-F′10-LF′20) received the Engineer degree in electrical engineering from the Universidad Tecnica Federico Santa Maria, in Valparaiso, Chile, in 1977 and the Dr.-Ing. degree in electrical engineering from the University of Erlangen, Erlangen, Germany, in 1985. He has been with the Department of Electronics Engineering, Universidad Tecnica Federico Santa Maria, since 1977, where he was full Professor and President. Since 2015 to 2019 he was the President of Universidad Andres Bello in Santiago, Chile. Since 2022 he is President of Universidad San Sebastian in Santiago, Chile. He has coauthored two books, several book chapters and more than 700 journal and conference papers. His main research interests include multilevel inverters, new converter topologies, control of power converters, and adjustable-speed drives. He has received a number of best paper awards from journals of the IEEE. Dr. Rodriguez is member of the Chilean Academy of Engineering. In 2014 he received the National Award of Applied Sciences and Technology from the government of Chile. In 2015 he received the Eugene Mittelmann Award from the Industrial Electronics Society of the IEEE. In years 2014 to 2021 he has been included in the list of Highly Cited Researchers published by Web of Science.